

1 Rethinking the role of transport and photochemistry in regional 2 ozone pollution: Insights from ozone concentration and mass budgets

3 Kun Qu^{1,2,3}, Xuesong Wang^{1,2}, Xuhui Cai^{1,2}, Yu Yan^{1,2}, Xipeng Jin^{1,2}, Mihalis Vrekoussis^{3,4,5}, Maria
4 Kanakidou^{3,6}, Guy Brasseur^{7,8}, Jin Shen⁹, Teng Xiao^{1,2}, Limin Zeng^{1,2}, and Yuanhang Zhang^{1,2,10,11}

5 ¹State Key Joint Laboratory of Environmental Simulation and Pollution Control, College of Environmental Sciences and Engineering,
6 Peking University, Beijing 100871, China

7 ²International Joint Laboratory for Regional Pollution Control, Ministry of Education, Beijing, 100816, China

8 ³Laboratory for Modeling and Observation of the Earth System (LAMOS), Institute of Environmental Physics (IUP), University of
9 Bremen, Bremen, Germany

10 ⁴Center of Marine Environmental Sciences (MARUM), University of Bremen, Germany

11 ⁵Climate and Atmosphere Research Center (CARE-C), The Cyprus Institute, Cyprus

12 ⁶Environmental Chemical Processes Laboratory, Department of Chemistry, University of Crete, Heraklion, Greece

13 ⁷Max Planck Institute for Meteorology, Hamburg, Germany

14 ⁸National Center for Atmospheric Research, Boulder, Colorado, USA

15 ⁹State Key Laboratory of Regional Air Quality Monitoring, Guangdong Key Laboratory of Secondary Air Pollution Research, Guangdong
16 Environmental Monitoring Center, Guangzhou 510308, China

17 ¹⁰Beijing Innovation Center for Engineering Science and Advanced Technology, Peking University, Beijing 100871, China

18 ¹¹CAS Center for Excellence in Regional Atmospheric Environment, Chinese Academy of Sciences, Xiamen 361021, China

19 *Correspondence to:* Xuesong Wang (xswang@pku.edu.cn) and Yuanhang Zhang (yhzhang@pku.edu.cn)

20 **Abstract.** Understanding the role of transport and photochemistry is essential to mitigate tropospheric ozone (O₃) pollution
21 within a region. In previous studies, the O₃ concentration budget has been widely used to determine the contributions of two
22 processes to the variations of O₃ concentrations. These studies often conclude that local photochemistry is the main cause of
23 regional O₃ pollution; however, they fail to explain why O₃ in a targeted region is often primarily derived from O₃ and/or its
24 precursors transported from the outside regions as reported by many studies of O₃ source apportionment. Here, we present a
25 method to calculate the hourly contributions of O₃-related processes to the variations of not only the mean O₃ concentration,
26 but also the total O₃ mass (the corresponding budgets are noted as the O₃ concentration and mass budget, respectively) within
27 the atmospheric boundary layer (ABL) of the concerned region. Based on the modelling results of WRF-CMAQ, the two O₃
28 budgets were applied to comprehensively understand the effects of transport and photochemistry on the O₃ pollution over the
29 Pearl River Delta (PRD) region in China. Quantified results demonstrate the different role of transport and photochemistry
30 when comparing the two O₃ budgets: Photochemistry drives the rapid increase of O₃ concentrations during the day, whereas
31 transport, especially vertical exchange through the ABL top, controls both rapid O₃ mass increase in the morning and decrease
32 in the afternoon. The diurnal changes of the transport contributions in the two O₃ budgets highlight the influences of the ABL
33 diurnal cycle and regional wind fields on regional O₃ pollution. ~~Although transport has a relatively limited effect on O₃
34 concentration compared to photochemistry, through high contributions to the O₃ mass increase in the morning, this
35 process~~transport determines that most O₃ in the PRD originates from the global background and emissions outside the region.
36 However, due to the simultaneous rapid increase of ABL volumes, this process only has a relatively limited effect on O₃

37 ~~concentration increase compared to photochemistry, and transport effect on the regional sources of O₃ cannot be illustrated by~~
38 ~~the O₃ concentration budget.~~ For future studies targeting O₃ and other secondary pollutants with moderately long atmospheric
39 lifetimes (e.g., fine particulate matter and some of its components), insights from both concentration and mass budgets are
40 required to fully understand the role of transport, chemistry and other related processes.

41 **1 Introduction**

42 Since first recognized as a key contributor to the Los Angeles smog, tropospheric ozone (O₃) pollution has received
43 considerable attentions in many highly populated areas in the world (Fishman et al., 2003; Schultz et al., 2017; Fleming et
44 al., 2018; Fowler et al., 2020). Exposure to O₃ threatens crop yields, ecosystems and human health, resulting in increased
45 mortality and economic losses (Mills et al., 2013; Ainsworth, 2017; Zhang et al., 2019). In addition, O₃ contributes to global
46 warming not only directly as a greenhouse gas, but also indirectly by damaging plants and suppressing land carbon sinks
47 (Sitch et al., 2007; Naik et al., 2021). To address these detrimental effects, efforts have been undertaken to reduce O₃ levels
48 in polluted regions. However, since O₃ is a secondary pollutant produced in the atmosphere by complex non-linear
49 chemistry, the abatement of O₃ pollution is a challenging task.

50

51 As a prerequisite to effectively control O₃ pollution, firstly, it is imperative to understand the effects of O₃-related processes
52 on the abundance of O₃ in the atmosphere. High O₃ concentrations within a region are often attributed to daytime
53 photochemical production from O₃ precursors, i.e. NO_x (= NO + NO₂) and volatile organic compounds (VOCs), under
54 sunlight. Due to the short lifetime of O₃ precursors (several hours for NO_x and reactive VOCs (Liu et al., 2016; Seinfeld and
55 Pandis, 2016; Laughner and Cohen, 2019)), it is generally believed that O₃ photochemistry is mainly linked to the
56 contributions of local emissions in polluted regions. On the other hand, since O₃ itself has a moderately long atmospheric
57 lifetime of 20-30 days (Stevenson et al., 2006; Bates and Jacob, 2019), transport processes in the atmosphere, including
58 horizontal transport (mainly advection) and vertical exchange through the top of the atmospheric boundary layer (ABL), may
59 also considerably contribute to regional O₃ pollution (Myriokefalitakis et al., 2016). Specifically, through vertical exchange,
60 O₃ in the residual layer and/or free atmosphere is entrained into the ABL and involved in the ABL mixing after sunrise,
61 leading to rapidly increasing O₃ concentrations near the surface (Kaser et al., 2017; Hu et al., 2018; Zhao et al., 2019).

62 Although O₃ produced from local emissions may be transported out ~~of~~ and later recirculated back to the region, it is more
63 likely that transported O₃ is mainly derived from the emissions of O₃ precursors in the upwind regions, continents and even
64 O₃ in the stratosphere under the combined effect of meso-, synoptic-, large- and global-scale atmospheric movements
65 (Massagué et al., 2019). If photochemistry has a comparatively large influence on O₃, ~~the reduction of~~reducing local
66 emissions is an appropriate strategy to alleviate regional O₃ pollution; otherwise, it is necessary to focus on emission control
67 in the upwind regions, aiming to reduce transport contributions to O₃.

68

69 In many studies, the O₃ concentration budget was often utilized to quantify the contributions of various transport and
70 chemical processes to the variations of O₃ concentrations. The changes in the mean O₃ concentration within the ABL ($\langle c_{O_3} \rangle$)
71 can be expressed as the net contributions of all O₃-related processes (Lenschow et al., 1981; Janssen and Pozzer, 2015; Vilà-
72 Guerau de Arellano et al., 2015):

$$\frac{\partial \langle c_{O_3} \rangle}{\partial t} = -\bar{u} \frac{\partial \langle c_{O_3} \rangle}{\partial x} - \bar{v} \frac{\partial \langle c_{O_3} \rangle}{\partial y} - \frac{\partial \overline{c_{O_3}' w'}}{\partial z} + S(O_3) \quad (1)$$

73 where u , v and w refer to wind speeds in the x-, y- and z-direction, respectively. The right side of Eq. (1) describes the
74 contributions of 1) horizontal transport (advection, the first two terms), 2) vertical exchange through the ABL top
75 (entrainment and detrainment, the third term), 3) gas-phase chemistry, dry deposition and other processes (the term $S(O_3)$)
76 indicates their net contributions). The O₃ concentration budget is then derived by integrating these terms over time. It enables
77 the identification of the processes that produce positive or negative tendencies of the O₃ concentration, and of the processes
78 that are most influential for regional O₃ pollution. Reported O₃ concentration budgets derived from ground-based
79 measurements (Su et al., 2018; Tan et al., 2018; Tan et al., 2019; Yu et al., 2020), aircraft-based mobile observations
80 (Lenschow et al., 1981; Trousdell et al., 2016; Trousdell et al., 2019) and Process Analysis (PA) or similar modules in
81 chemical transport models (Hou et al., 2014; Li et al., 2021; Yan et al., 2021) in various regions of the globe often suggest
82 that O₃ production through local photochemistry drives the noon-time increase of O₃ concentration, whereas transport
83 reduces O₃ concentration over the same period. Conclusively, photochemistry, rather than transport, plays a main role in O₃
84 pollution.

85
86 However, O₃ source apportionment is likely to provide different conclusions about the relative importance of transport and
87 photochemistry in affecting O₃ pollution. O₃ source apportionment is performed to identify the regional and/or sectoral
88 origins of O₃, of which the results are also used to support air pollution control (Clappier et al., 2017; Thunis et al., 2019).
89 Here, we only discuss the regional origins of O₃, because the contributions of sources outside the region (or emissions within
90 the region, defined as local emissions hereafter) provide information on the influence of transport (or photochemistry) on O₃
91 pollution. Previous publications often conclude that most O₃ was not derived from ~~the~~ local emissions of O₃ precursors, but
92 from the global background and emissions outside the targeted regions (Guo et al., 2018; Pay et al., 2019; Liu et al., 2020).
93 The mixing ratios of background O₃ in various regions of the world are mostly within the range of 30-50 ppb (Reid et al.,
94 2008 and references therein), which are sufficiently high to ensure that O₃ originates mainly from non-local sources in less
95 polluted regions. Since controlling background O₃ is challenging, efforts to control O₃ pollution in polluted regions with high
96 non-local contributions to O₃ should focus on reducing emissions ~~from~~ in upwind regions rather than only local areas
97 (Lelieveld et al., 2009; Boian and Andrade, 2012; Massagué et al., 2019). One successful example is the establishment of the
98 “Ozone Transport Region” in the north-eastern United State by the US Environmental Protection Agency, which promotes
99 collaborative emission reductions among states to address inter-state O₃ transport (Novel, 1992). The above discussion
100 highlights the importance of transport for regional O₃ pollution, since it often plays a more prominent role than local

101 photochemistry. Apparently, this last statement conflicts with the conclusions derived from the O₃ concentration budget.
102 Thus, while the O₃ concentration budget is useful for understanding O₃ pollution, it may not completely illustrate the effects
103 of transport and photochemistry on regional O₃ pollution.

104

105 In the ABL of the concerned region, the mean O₃ concentration and total O₃ mass are both conserved, which means that their
106 variations are equal to the net contributions by various O₃-related processes including transport and photochemistry. These
107 relationships can be represented by the O₃ concentration budget and mass budget, respectively. Unlike the aforementioned
108 O₃ concentration budget in Eq. (1), the hourly O₃ mass budget, written as

$$\frac{\partial m_{O_3}}{\partial t} = -(\bar{u}s_x\langle c_{O_3} \rangle + \bar{v}s_y\langle c_{O_3} \rangle) - \overline{c_{O_3}'w'}s_z + S(O_3)V \quad (2)$$

109 is seldom reported (m_{O_3} is the total O₃ mass within the ABL of the region; s_x , s_y , s_z are the areas of the interfaces in the x-,
110 y- and z-direction, respectively; V is the volume of the ABL column). Due to the varied effects of transport on O₃
111 concentration and mass, the O₃ mass budget differs from the O₃ concentration budget but is more suitable to explore the
112 influence of transport and photochemistry on the results of O₃ source apportionment (more detailed explanations are given in
113 Sect. 2.4). In order to comprehensively understand the role of transport and photochemistry in regional O₃ pollution, in the
114 present study, we developed a method to calculate both the O₃ concentration and mass budget based on the simulation results
115 from the Weather Research and Forecasting (WRF) and Community Multiscale Air Quality (CMAQ) models, and also
116 analysed, compared the results of the two regional-level O₃ budgets. The Pearl River Delta (PRD) region, a city cluster
117 located on the southeast coast of China and exposed to severe O₃ pollution in summer and autumn (Gao et al., 2018), was
118 selected as the targeted region. The tasks for this study can be summarized as follows:

119

120 *1) Development of the method to quantify the two O₃ budgets*

121 WRF-CMAQ employs the Process Analysis (PA) module to assess the contributions of O₃-related processes to the variations
122 of O₃ concentrations within each grid cell. However, to obtain the regional-level O₃ concentration and mass budgets, the
123 results of PA module are not sufficient. One reason is that the contribution of vertical exchange through the ABL top is not
124 specifically quantified in commonly used ABL parameterizations, thus requires additional calculations (Kaser et al., 2017).
125 Additionally, calculations based on the PA results are needed to identify the contributions of other O₃-related processes to
126 ABL-mean O₃ concentration as well as the results of the O₃ mass budget. To address this, we developed a method to quantify
127 the two O₃ budgets, of which the details are given in Sect. 2.1-2.3.

128

129 *2) Analysis and comparison of the results from the two O₃ budgets*

130 Based on the simulations of O₃ pollution in the PRD with the model setup introduced in Sect. 2.5, the two O₃ budgets were
131 calculated for further analyses and comparisons to reveal the role of transport and photochemistry in regional O₃ pollution
132 from a more comprehensive perspective. Relative discussions are presented in Sect. 3.

133

134 *3) Assessment of the role of transport and photochemistry in determining the regional origins of O₃*

135 The Brute Force Method (BFM; Clappier et al., 2017), a widely used source apportionment method, was combined with the
136 O₃ mass budget calculation to determine the contributions of emissions within and outside the PRD as well as background
137 sources to the O₃ transported into or produced by photochemistry in the region (methodology described in Sect. 2.6). The
138 results, as discussed in Sect. 4, reveal the impacts of transport and photochemistry in determining the regional origins of O₃
139 in the PRD, and explain why the different views on the role of two processes in regional O₃ pollution are suggested by the O₃
140 concentration budget and O₃ source apportionment studies.

141 **2 Methodology: O₃ budget calculations and model setup**

142 **2.1 The PRD grids and O₃-related processes in O₃ budgets**

143 The two O₃ budgets were calculated for the PRD, of which the grids are shown in the lower-left panel of Fig. 1. These grids
144 are set based on the finer modelling domain of WRF-CMAQ (details given in Sect. 2.5) and determined according to the
145 administrative areas of the PRD. The PRD grids with one or several interfaces with the outer regions are defined as the
146 border grids, and they can be further classified as the grids in the north, south, west and east borders based on their locations.
147 Correspondingly, the PRD grids with no interface with the outer regions are defined as the non-border grids.

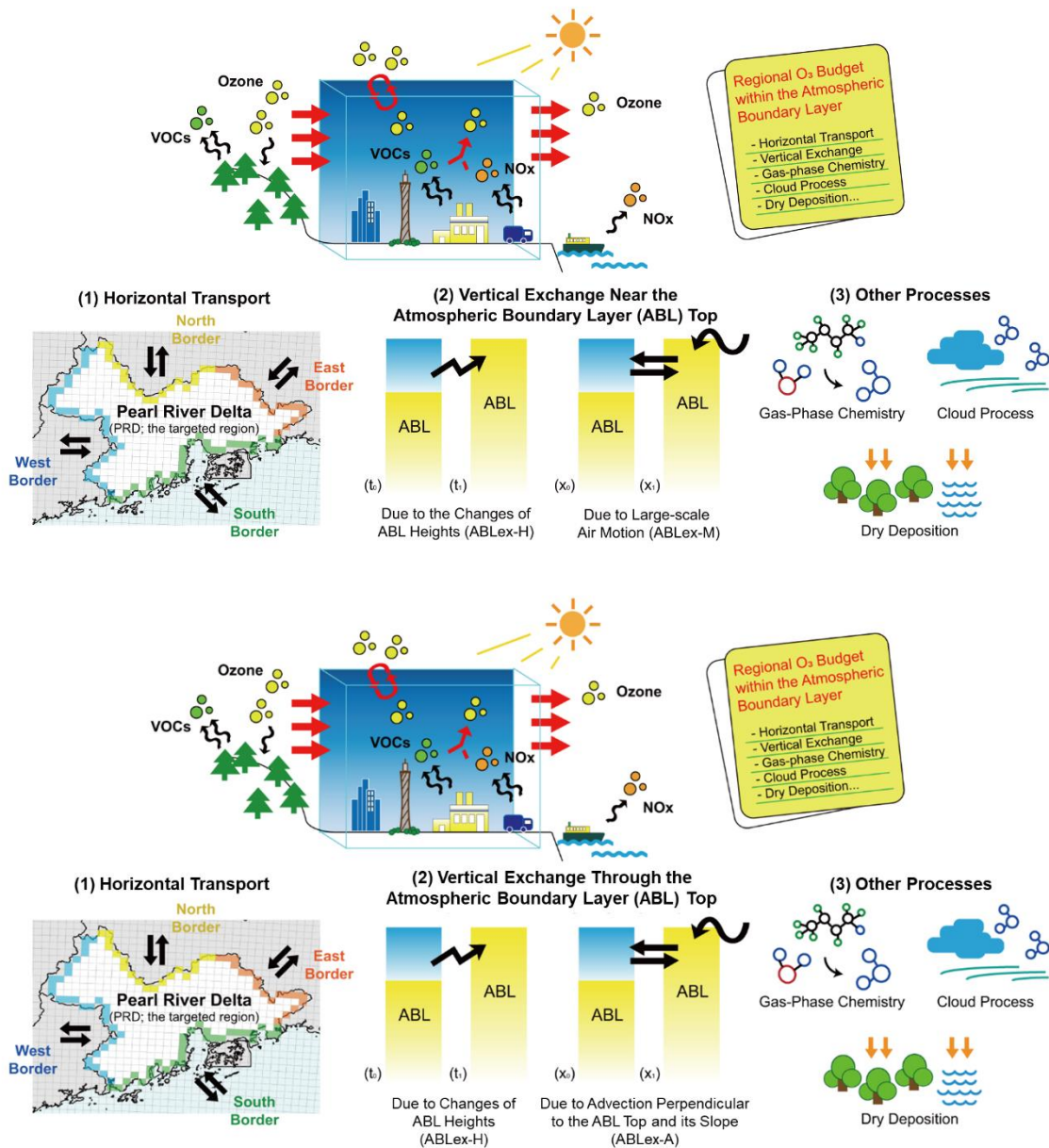
148

149 Figure 1 also displays all O₃-related processes considered in the calculation of O₃ budgets here. The transport processes
150 include horizontal transport through the four types of borders and vertical exchange through the ABL top. For vertical
151 exchange, its contribution in the O₃ concentration budget (the third term on the right side of Eq. (1)) is quantified by (Sinclair
152 et al., 2010; Jin et al., 2021):

$$-\frac{\partial \overline{c_{O_3}' w'}}{\partial z} = \frac{\Delta c_{O_3}}{H} \frac{\partial H}{\partial t} + \frac{\Delta c_{O_3}}{H} \left(u_h \frac{\partial H}{\partial x} + v_h \frac{\partial H}{\partial y} - w_h \right) \quad (3)$$

153 where H is the ABL height; Δc_{O_3} is the difference between O₃ concentrations above and within the ABL; u_h , v_h and w_h are
154 the ABL-top wind speeds in the x, y and z-direction, respectively. The terms on the right side of Eq. (3) suggest that ~~the~~
155 ~~occurrence of~~ vertical exchange through the ABL top, or entrainment and detrainment, is attributed to 1) the temporal
156 changes of ABL heights (H) and 2) ~~large-scale air motion~~ (advection) perpendicular to the ABL top and its slope. For the
157 convenience of discussion, hereafter, vertical exchanges due to the above two dynamic processes are marked as ABLex-H
158 and ABLex-~~MA~~, respectively. The contributions of all transport processes in the O₃ budgets were quantified based on
159 meteorological parameters simulated by WRF and O₃ concentrations simulated by CMAQ. The basic calculations of the
160 contributions from the above-mentioned transport processes in the O₃ mass and concentration budgets are separately
161 introduced in the following two sections.

162



163

164

165 **Figure 1.** Schematic illustration of O₃ budgets (the upper panel) and O₃-related processes considered (the lower panel): (1) Horizontal
 166 transport through the north, south, west and east borders of the Pearl River Delta (PRD) (the distributions of the PRD grids are also shown:
 167 yellow, green, blue, orange for the north, south, west and east border grids, respectively, and white for the non-border grids); (2) Vertical
 168 exchange through the atmospheric boundary layer (ABL) top, including the process due to the changes of ABL heights (ABLex-H) and
 169 large scale air motion advection perpendicular to the ABL top and its slope (ABLex-A); (3) Other processes, including gas-phase
 170 chemistry, cloud process and dry deposition ~~in~~for this study.

171

172 Other processes in the O₃ budgets include gas-phase chemistry (including daytime photochemical O₃ production, O₃ titration
 173 by NO and O₃ depletion with unsaturated VOCs, etc.), cloud process (including below and in-cloud mixing, aqueous-phase
 174 chemistry, wet deposition; Liu et al., 2011) and dry deposition. The contributions of these processes are all calculated based
 175 on the output of the PA module in CMAQ. In a word, their contributions in the O₃ mass budget are obtained by summing up
 176 the contributions in all grid cells within the ABL of the PRD, and their contributions in the O₃ concentration budget are the
 177 corresponding contributions to O₃ mass divided by the volume of the ABL of the PRD. Since diffusion through the side and
 178 top boundaries of the region is expected to have a negligible influence on the variations of both O₃ concentration and mass,
 179 we did not consider this process in O₃ budget calculations.

180

181 The calculation process of the two O₃ budgets is summarized as follows. Based on multiple output files of WRF and CMAQ,
 182 firstly, the contributions of all considered O₃-related processes to O₃ mass changes and volumes-/volume changes linked to
 183 these processes within the ABL are calculated nearly-in nearly all grid ~~columns~~ of the modelling domain. We developed the
 184 post-processing tool *flux_4d_cal* to conduct the above calculations. Afterwards, the regional-level O₃ mass and concentration
 185 budgets are quantified based on the results of the first-step calculations. Particularly, the method described in Sect. 2.3 is
 186 applied to estimate the contributions of O₃-related processes in the O₃ concentration budget. More detailed descriptions of
 187 the calculation process can be found in Text S1.

188 2.2 Transport contributions in the O₃ mass budget

189 The method by Yang et al. (2012) and Chang et al. (2018) was applied to quantify the contributions of horizontal transport in
 190 the O₃ mass budget. For instance, the contribution of the advection through the west/east interface of a grid ~~cell~~ column
 191 within the ABL to total O₃ mass (F_{htrans}) in the column during the time interval dt is calculated as:

$$F_{htrans} = \int_0^H c_{O_3} u L dz dt \quad (4)$$

192 where L is the width of the grid ~~cell~~ (equal to the horizontal resolution in the model); dz is the height of vertical layers. For
 193 advection through the north/south interface, the calculation is similar to Eq. (4), except for using v instead of u . F_{htrans}
 194 values through all interfaces between the border grids and the outer region were calculated. Afterwards, they are summed up
 195 separately according to the types of borders as the net contributions of horizontal transport through the north, south, west and
 196 east borders of the PRD in the O₃ mass budget.

197

198 Following Sinclair et al. (2010) and Jin et al. (2021), the contribution of vertical exchange through the ABL top to O₃ mass
 199 (F_{ABLex}) during the time interval dt can be expressed as:

$$\begin{aligned} F_{ABLex} &= F_{ABLex-H} + F_{ABLex-MA} \\ &= c_{O_3-h} \frac{\partial H}{\partial t} L^2 dt + c_{O_3-h} \left(u_h \frac{\partial H}{\partial x} + v_h \frac{\partial H}{\partial y} - w_h \right) L^2 dt \end{aligned} \quad (5)$$

200 where $c_{O_3,h}$ is the O_3 concentration at the ABL top. The two terms on the right-most side of Eq. (5) separately describe the
 201 contributions of ABLex-H and ABLex-~~M-A~~ (denoted separately as $F_{ABLex-H}$ and $F_{ABLex-MA}$). F_{ABLex} values in all the ~~ABL~~
 202 ~~top~~ grids over the PRD were summed up to derive the net contribution of vertical exchange through the ABL top in the O_3
 203 mass budget.

204 2.3 Transport contributions in the O_3 concentration budget

205 It is difficult to directly apply Eq. (1) in the quantification of transport contributions in the regional-level O_3 concentration
 206 budget. Therefore, a different approach was applied, which is introduced as follows.

207

208 Suppose that an air parcel with a total volume of dV is transported into the ABL of the PRD (its original volume is V) ~~during~~
 209 ~~the time interval dt~~ . The variation of $\langle c_{O_3} \rangle$ under the influence of horizontal transport ($d\langle c_{O_3} \rangle_{htrans}$) can be written as:

$$d\langle c_{O_3} \rangle_{htrans} = \frac{F_{htrans} + \langle c_{O_3} \rangle (V - dV)}{V} - \langle c_{O_3} \rangle = \frac{F_{htrans} - \langle c_{O_3} \rangle dV}{V} \quad (6)$$

210 Since ABLex-~~M-A~~ is also an advection process, its contribution in the O_3 concentration budget ($d\langle c_{O_3} \rangle_{ABLex-MA}$) can be
 211 quantified using a similar formula as Eq. (6), except for using $F_{ABLex-MA}$ instead of F_{htrans} .

212

213 Through ABLex-H, air parcels in the residual layer and/or free atmosphere are merged into the ABL or vice versa. Thus, the
 214 variation of $\langle c_{O_3} \rangle$ under its influence ($d\langle c_{O_3} \rangle_{ABLex-H}$) is expressed as:

$$d\langle c_{O_3} \rangle_{ABLex-H} = \frac{F_{ABLex-H} + \langle c_{O_3} \rangle V}{V + dV} - \langle c_{O_3} \rangle = \frac{F_{ABLex-H} - \langle c_{O_3} \rangle dV}{V + dV} \quad (7)$$

215

216 If the targeted region is small enough, the expressions of $d\langle c_{O_3} \rangle_{htrans}$ and $d\langle c_{O_3} \rangle_{ABLex-H}$ in Eqs. (6) and (7) can be
 217 transformed to the corresponding terms in Eq. (1), confirming the applicability of the above calculations (for details, see
 218 Text S2). All variables in Eqs. (6) and (7) can be quantified by the post-processing tool *flux_4d_cal*, making the method
 219 feasible and suitable for the afterward calculations of the regional-scale O_3 concentration budget.

220

221 However, due to the prominent diurnal cycle of ABL, V in Eqs. (6) and (7) may change notably within an hour, leading to
 222 bias in the hourly estimations of $d\langle c_{O_3} \rangle_{htrans}$, $d\langle c_{O_3} \rangle_{ABLex-H}$ and $d\langle c_{O_3} \rangle_{ABLex-MA}$ when using V at the start and end of the
 223 hour. This problem also applies to the calculation of contributions from other O_3 -related processes. In order to reduce the
 224 potential bias caused by the different selections of V , we designed two calculation paths for the hourly O_3 concentration
 225 budget (Fig. S1):

226

- O_3 mass change \rightarrow ABL volume change

227

- ABL volume change \rightarrow O_3 mass change

228 where only O₃ mass or ABL volume changes in each calculation step. The contribution of ABLex-H to O₃ concentration can
 229 be viewed as the net effects of ABL volume change and O₃ being transported into/out of the ABL: ABL volume change due
 230 to ABL development (collapse) leads to lower (higher) O₃ concentration, and O₃ transported into (out of) the ABL through
 231 ABLex-H leads to O₃ increase (decrease). These contributions are quantified separately in the ABL volume and O₃ mass
 232 change step. The contributions of horizontal transport, ABLex-~~M~~A and non-transport processes are quantified only in the O₃
 233 mass change step. The contribution of each process to the variation of O₃ concentration is calculated using both paths, and
 234 the mean value of two results serves as an estimation close to its real contribution in the O₃ concentration budget.

235 2.4 Difference between the two O₃ budgets

236 The difference between the two O₃ budgets is linked to the varied effects of transport on O₃ mass and concentration. Suppose
 237 that the mean O₃ concentration in the transported air parcels is $\langle c_{O_3} \rangle_{trans}$. For horizontal transport, its contributions in the O₃
 238 mass and concentration budgets can be separately written as:

$$F_{htrans} = \langle c_{O_3} \rangle_{trans} dV \quad (8)$$

$$d\langle c_{O_3} \rangle_{htrans} = \frac{dV}{V} (\langle c_{O_3} \rangle_{trans} - \langle c_{O_3} \rangle) \quad (9)$$

239 Apparently, F_{htrans} is related to the O₃ concentrations in the transported air parcels, but not to those in the studied region. It
 240 indicates ~~how much~~the amount of O₃ ~~mass is~~ transported into or out of the region. Whether it is positive or negative only
 241 depends on the direction of transport — O₃ being transported into (out of) the region leads to the increase (decrease) of O₃
 242 mass, which corresponds to a positive (negative) contribution in the O₃ mass budget. In contrast, $d\langle c_{O_3} \rangle_{htrans}$ quantifies how
 243 much horizontal transport alters regional-mean O₃ concentrations, and is linked to the difference between O₃ concentrations
 244 in the transported air parcels and the studied region (Eq. (9)). O₃ being transported into (out of) the region does not
 245 necessarily result in a higher (lower) O₃ concentration. For instance, when clean air parcels with relatively low O₃ levels are
 246 transported into the region, they dilute O₃ pollution and reduce O₃ concentration ($d\langle c_{O_3} \rangle_{htrans} < 0$). Given that ABLex-~~M~~A
 247 is also an advection process, the above difference also applies to this process ~~as well~~. For ABLex-H, its contributions in the
 248 O₃ mass and concentration budgets are expressed as:

$$F_{ABLex-H} = \langle c_{O_3} \rangle_{trans} dV \quad (10)$$

$$d\langle c_{O_3} \rangle_{ABLex-H} = \frac{dV}{V + dV} (\langle c_{O_3} \rangle_{trans} - \langle c_{O_3} \rangle) \quad (11)$$

249 Similarly, ABL development and collapse lead to the increase and decrease of O₃ mass, respectively, but whether they
 250 contribute to higher or lower O₃ concentration also depends on the difference between O₃ concentration in the transported air
 251 parcels and that in the region. Based on the above discussion, these transport processes all show different effects on O₃ mass
 252 and concentration — the effect of transport on the variations of O₃ mass is only related to the characteristics of the
 253 transported air parcels, namely their volumes and O₃ concentrations within (Eqs. (8) and (10)), while how transport

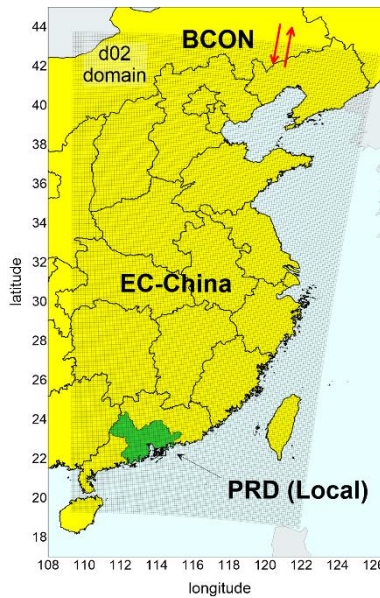
254 contributes to the variations of O₃ concentration is linked to the difference between O₃ concentrations in the transported air
255 parcels and the region (Eqs. (9) and (11)).

256

257 To properly analyse the impact of transport and photochemistry on the regional origins of O₃, it is required to identify the
258 regional origins of the “new O₃” into the studied region and the “disappeared O₃” out of the studied region contributed by
259 various O₃-related processes, rather than how these processes lead to the variations of O₃ concentration. Thus, the influence
260 of transport and photochemistry on the results of O₃ source apportionment can be ~~shown~~explored by the O₃ mass budget, but
261 not by the O₃ concentration budget. By utilizing the BFM source apportionment method in combination with the O₃ mass
262 budget calculation, we can identify the regional origins of O₃ mass increase and decrease due to transport and
263 photochemistry, and explain how these processes determine the results of O₃ source apportionment in the PRD.

264 **2.5 Model setup and validation**

265 The O₃ concentration and mass budgets within the ABL of the PRD were calculated based on the WRF-CMAQ modelling
266 results by Qu et al. (2021a). The WRF (version 3.2) and CMAQ (version 5.0.2) models were used to simulate the
267 meteorological and pollutant fields, respectively. Two domains with the resolution of 36 and 12 km (denoted as d01 and d02
268 hereafter) were set up for the one-way nested simulations, and the results in the finer d02, which includes the PRD and most
269 areas in East and Central China (Fig. 2), were used in the calculations of O₃ budgets. To represent the contributions of global
270 background to O₃, the initial and boundary conditions for the coarse d01 domain were provided from the global model, the
271 Model for Ozone and Related Chemical Tracers, version 4 (MOZART-4). The PRD inventory provided by the Guangdong
272 Environmental Monitoring Centre, the Multi-resolution Emission Inventory for China (MEIC) inventory for the mainland
273 China (He, 2012), the MIX inventory for the Asian regions outside of mainland China (Li et al., 2017) and biogenic
274 emissions simulated by the Model of Emissions of Gases and Aerosols from Nature (MEGAN; version 2.10) model were
275 used in the simulations. SAPRC07 (Carter, 2010) and AERO6 were applied as the gas-phase chemistry mechanism and the
276 aerosol scheme, respectively. The simulations of O₃ pollution in the PRD were performed for October 2015 (October 11–
277 November 10, 2015) and July 2016 (July 1–31, 2016), which ~~were selected~~serve as the representative months in autumn and
278 summer, respectively. Here, O₃ polluted days are defined when the maximum hourly O₃ concentrations of the day exceed
279 200 µg/m³, or the maximum 8-hour average O₃ concentrations of the day exceed 160 µg/m³ (both are the Grade-II O₃
280 thresholds in the Chinese National Ambient Air Quality Standard) in any municipality of the PRD. According to this
281 definition, there were 16 and 12 O₃ polluted days in the two months, respectively (more information is given in Table S1).
282 The mean O₃ budgets during these O₃ polluted days of two seasons were separately calculated and discussed in the present
283 study.



284

285 Figure 2. The spatial distributions of the d02 modelling domain and source regions. The d02 domain is displayed as the nested areas in the
 286 figure. PRD, Pearl River Delta; EC-China, East and Central China; BCON, the boundary conditions of d02 modelling, or the contributions
 287 of sources outside the d02 domain.
 288

289 We evaluated the performance of WRF-CMAQ modelling based on multiple observational datasets. The modelling results of
 290 meteorological parameters (including temperature, relative humidity and wind speed), O₃, NO₂ concentrations and the
 291 mixing ratios of hydrocarbons were validated with corresponding observations in the PRD by Qu et al. (2021a). The
 292 performance of the model ~~to simulate~~ in simulating the above variables was overall satisfying with low biases and high
 293 correlations (for details, see Qu et al., 2021a). In this study, we further compared the modelled ABL height, the vertical
 294 profiles of wind speed, direction and O₃ mixing ratio in Hong Kong (located in the south PRD) with ~~the~~ corresponding
 295 observations from the IAGOS (In-service Aircraft for a Global Observing System; Petzold et al., 2015) dataset. The
 296 modelled ABL heights showed similar hourly variations during the day as the observational results (R = 0.76), with a mean
 297 bias of -1.1 m (Fig. S2). The mean biases of mean wind speeds are within the range of ± 1 m/s in all considered height
 298 ranges (0-1 km, 1-2 km, 2-5 km), and the results of the IAGOS and WRF model indicate similar variations of prevailing
 299 wind directions in different seasons and height ranges (Fig. S3). Moreover, modelled O₃ mixing ratios in Oct. 2015 are
 300 overestimated by 6% and 26% in the height range of 0-1 km and 1-2 km, respectively, and sufficiently illustrate the
 301 development, maintenance and dissipation of O₃ pollution during the month (Fig. S4). More detailed evaluations on the
 302 model performance of these parameters are presented in Text S3 of the Supplement. Overall, the model performance is
 303 acceptable, indicating that the model can provide reasonable data for the calculations of O₃ budgets.

304

305 If the calculation methods and assumptions are reasonable, the conservation of O₃ concentration and mass budgets, described
306 as

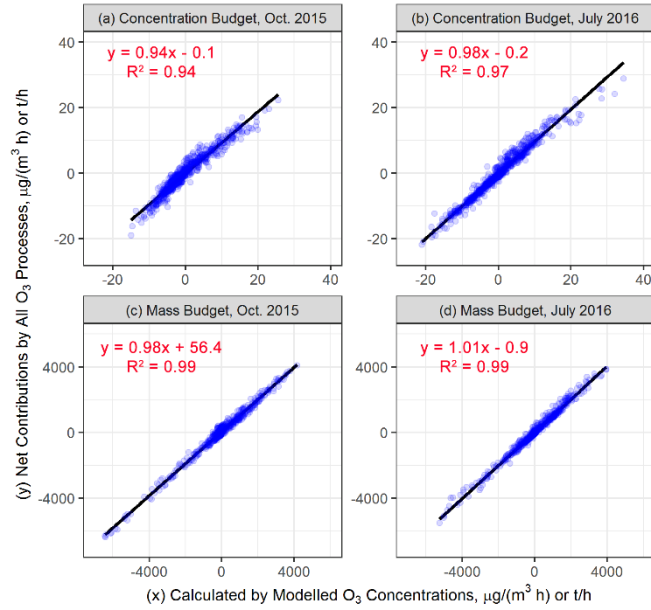
$$\frac{\partial \langle c_{O_3} \rangle (or m_{O_3})}{\partial t} - (S_{htrans} + S_{ABLex} + S_{chem} + S_{cloud} + S_{ddep}) = 0 \quad (12)$$

307 can be achieved (the terms S_{htrans} , S_{ABLex} , S_{chem} , S_{cloud} and S_{ddep} indicate the contributions of horizontal transport, vertical
308 exchange through the ABL top, gas-phase chemistry, cloud process and dry deposition, respectively, in the O₃ concentration
309 or mass budgets). Therefore, we used Eq. (12) to examine the validity of the O₃ budget calculations. Total O₃ masses at the
310 start and end of each hour were directly used to calculate the hourly variations of O₃ mass ($\frac{\partial m_{O_3}}{\partial t}$). Besides these two
311 parameters, the volumes of the ABL of the PRD at the start and end of each corresponding hour (calculated using ABL
312 heights in all the PRD grids) are also needed to calculate the hourly variations of O₃ concentration ($\frac{\partial \langle c_{O_3} \rangle}{\partial t}$). The contributions
313 of various O₃-related processes in the O₃ concentration and mass budgets were quantified using the method introduced in
314 Sect. 2.1-2.3. As displayed in Fig. 23, hourly variations of O₃ concentration/mass and the corresponding net contributions
315 from all O₃-related processes show good correlations ($R^2 > 0.9$), with all fitted lines close to the 1:1 line. Thus, the
316 conservation is overall met for the two O₃ budgets in both representative months, allowing for further analyses based on the
317 quantified budgets.

318 2.6 Identifying regional origins of O₃ mass changes due to transport and photochemistry

319 The question to be addressed is how O₃-related processes determine the regional origins of O₃. By combining the O₃ mass
320 budget calculations with the BFM source apportionment method, we identified the regional origins of O₃ mass changes due
321 to transport and photochemistry (gas-phase chemistry). Here, the ~~Of~~ interest ~~were~~ lies in the contributions of emissions in the
322 PRD (also defined as local emissions), in other regions within d02 (mainly East and Central China, hereafter denoted as EC-
323 China), and in regions outside the d02 (the boundary conditions (BCON) of d02 modelling; representative of the background
324 sources). The distribution of these source regions is shown in Fig. 52. Besides the base scenario where all emissions in d02
325 were considered in simulations, three sensitivity scenarios were additionally simulated:

- 326 • The PRD_zero scenario: All emissions (including anthropogenic and biogenic emissions; the same below) in the
327 PRD were zeroed out;
- 328 • The EC-China_zero scenario: All emissions in the EC-China were zeroed out;
- 329 • The All_zero scenario: All emissions within d02 were shut down.



330

331 **Figure 23.** The examinations of O₃ budget conservation in Oct. 2015 (a,c) and July 2016 (b,d) for the hourly O₃ concentration budget (a-b)
 332 and mass budget (c-d). The units for the O₃ concentration and mass budgets are µg/(m³ h) and t/h, respectively. The solid black lines in the
 333 plots are the fitted lines.

334 The hourly contributions of the process *i* in the O₃ mass budget were quantified using the same method outlined in Sect. 2.1-
 335 2.2 for the base scenario and three sensitivity scenarios, denoted as $f_{i,base}$, f_{i,PRD_zero} , $f_{i,EC-China_zero}$, and f_{i,all_zero} ,
 336 respectively. These parameters enable the determination of the contributions of emissions from the PRD and EC-China as
 337 well as the background sources (BCON) to the O₃ mass increase and decrease due to various O₃-related processes. The
 338 contributions of BCON in the O₃ mass changes due to the process *i* ($F_{i,BCON}$) can be estimated directly as the contributions of
 339 the process *i* to the O₃ mass in the All_zero scenario:

$$F_{i,BCON} = f_{i,all_zero} \quad (13)$$

340 For the contributions of the PRD and EC-China emissions from the process *i* (separately denoted as $F_{i,PRD}$ and $F_{i,EC-China}$),
 341 they can be derived in two ways: 1) by subtracting simulations with zeroed studied emissions from the base case simulation
 342 (top-down BFM); 2) by subtracting simulations without all emissions from simulations accounting only for studied
 343 emissions (bottom-up BFM). Due to the non-linear response of O₃ to precursor emissions, the results from top-down and
 344 bottom-up BFM can differ, which may lead to the non-additivity of the results (the sum of all contributions is not equal to
 345 the concerned metric; here, $F_{i,PRD} + F_{i,EC-China} + F_{i,BCON} \neq f_{i,base}$). Therefore, we estimated $F_{i,PRD}$ and $F_{i,EC-China}$ as the
 346 average values of the contributions by using top-down BFM and bottom-up BFM:

$$F_{i,PRD} = \frac{1}{2} [(f_{i,base} - f_{i,PRD_zero}) + (f_{i,EC-China_zero} - f_{i,all_zero})] \quad (14)$$

$$F_{i,EC-China} = \frac{1}{2}[(f_{i,base} - f_{i,EC-China_zero}) + (f_{i,PRD_zero} - f_{i,all_zero})] \quad (15)$$

347 It should be noted that to identify the origins of both “new O₃” into the region and “disappeared O₃” out of the region, the
 348 positive and negative contributions of O₃-related processes to the O₃ mass in the PRD grids were separately summed up for
 349 the base and sensitivity scenarios and quantified using Eqs. (13-15).

350 3 Analyses and comparisons of O₃ concentration and mass budget

351 3.1 O₃ concentration budget

352 The upper panels of Fig. 3-4 show the mean diurnal changes of the O₃ concentration budget within the ABL of the PRD.
 353 According to the net contributions from all O₃-related processes considered, ABL-mean O₃ concentration increased during
 354 most hours in the daytime, with the highest rates occurring in the early morning (8:00-10:00 local time (LT) in autumn, 7:00-
 355 9:00 LT in summer). The reduction of ABL-mean O₃ concentration in the late afternoon and at night was also considerable.
 356 Its rate reached the maximum values near the sunset time (~18:00 LT in autumn, ~19:00 LT in summer) and gradually
 357 decreased throughout the night. The following question is then raised on the suitability of the budget targeting on ABL-mean
 358 O₃ concentration to explain the variations of O₃ concentrations near the ground. To answer this question, we compared the
 359 hourly changes of modelled ABL-mean O₃ concentration with those of observed and modelled mean near-surface O₃
 360 concentrations in 18 sites of the Guangdong-Hong Kong-Macao PRD Regional Air Quality Monitoring Network
 361 (distributions shown in Fig. S6S5). As presented in Fig. S7S6, these datasets display similar patterns of O₃ diurnal changes.
 362 Since O₃ was well mixed within the ABL (Fig. S4), especially during daytime when O₃ levels are higher than those at night,
 363 the budget of ABL-mean O₃ concentration can reveal the influences of transport and photochemistry on the variations of
 364 overall O₃ levels as well as the causes of O₃ pollution in the targeted region.

365

366 Next, the contributions of various O₃-related processes in the O₃ concentration budget are discussed as follows:

- 367 • Gas-phase chemistry: Figure 3-4 shows that gas-phase chemistry controlled almost exclusively the O₃ concentration
 368 budget. During the morning hours, which are defined as the period from sunrise (~6:00 LT in autumn, ~5:00 LT in
 369 summer) to the O₃-peak hour (~14:00 LT), gas-phase chemistry (photochemistry) contributed to, on average, 74%
 370 and 95% of the O₃ concentration increase in autumn and summer, respectively. These contributions are notably
 371 higher than the contributions of transport in the same periods (25% in autumn, 5% in summer). In the afternoon,
 372 gas-phase chemistry was still the main process to maintain high O₃ concentrations within the PRD, but its
 373 contributions gradually decreased ~~until sunset~~. However, this process led to decreased O₃ concentration at night,
 374 suggesting the impact of O₃ titration by emitted NO and O₃ depletion with unsaturated VOCs. It may also be related
 375 to the production of particle nitrate through N₂O₅ hydrolysis (Qu et al., 2021b).

- 376
- 377
- 378
- 379
- 380
- 381
- 382
- 383
- 384
- 385
- 386
- 387
- 388
- Transport: The dominance of gas-phase chemistry in the O₃ concentration budget does not mean that the influence of transport on O₃ concentration can be neglected all day long. Considerable contributions of transport (mainly by ABLex-H) to O₃ concentration increase are found during 2-3 hours after sunrise, with the highest hourly mean contributions reaching ~40% and ~25% in autumn and summer, respectively. This result indicates the notable influence of air masses with high O₃ concentrations being entrained from residual layers on near-surface O₃ pollution. ABLex-~~M~~A and horizontal transport may contribute to the increase or decrease of ABL-mean O₃ concentration, depending on the O₃ levels in air parcels transported into and out of the region (further analysis is provided in Sect. 3.3). Overall, these two transport processes had only limited contributions to the variations of O₃ concentration.
 - Other processes: Dry deposition contributed to a considerable decrease in O₃ concentration, especially during daytime, and thus served as an important sink process for near-surface O₃. Besides, cloud process was also an important sink process for O₃ in summer, which might be related to the convective vertical transport of O₃.

389 In summary, the results of the O₃ concentration budget indicate that gas-phase chemistry played a major role in the variations

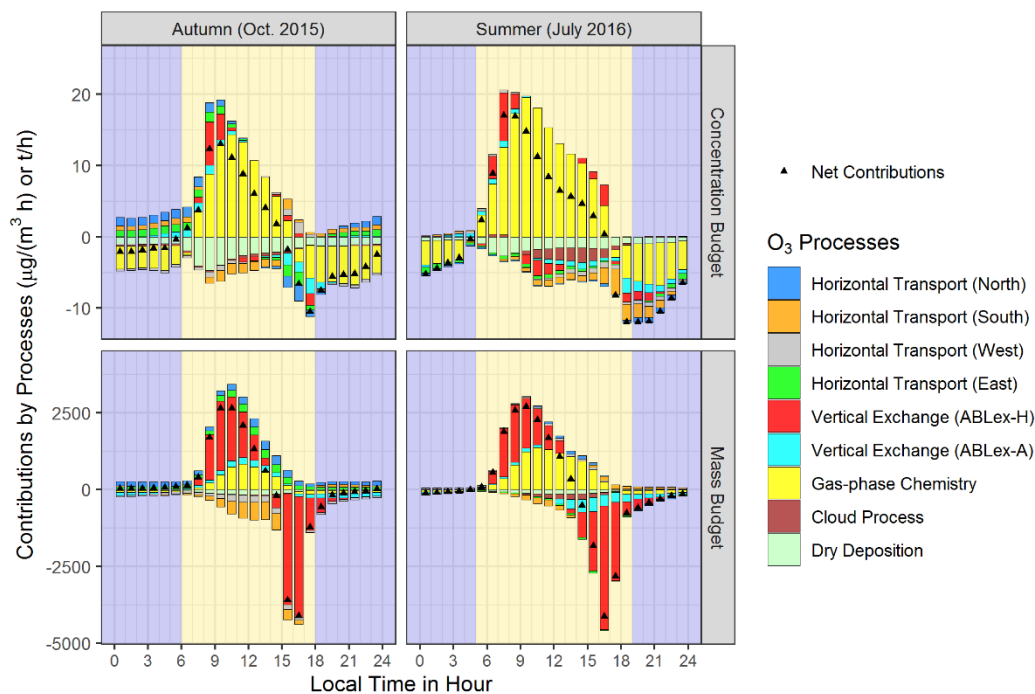
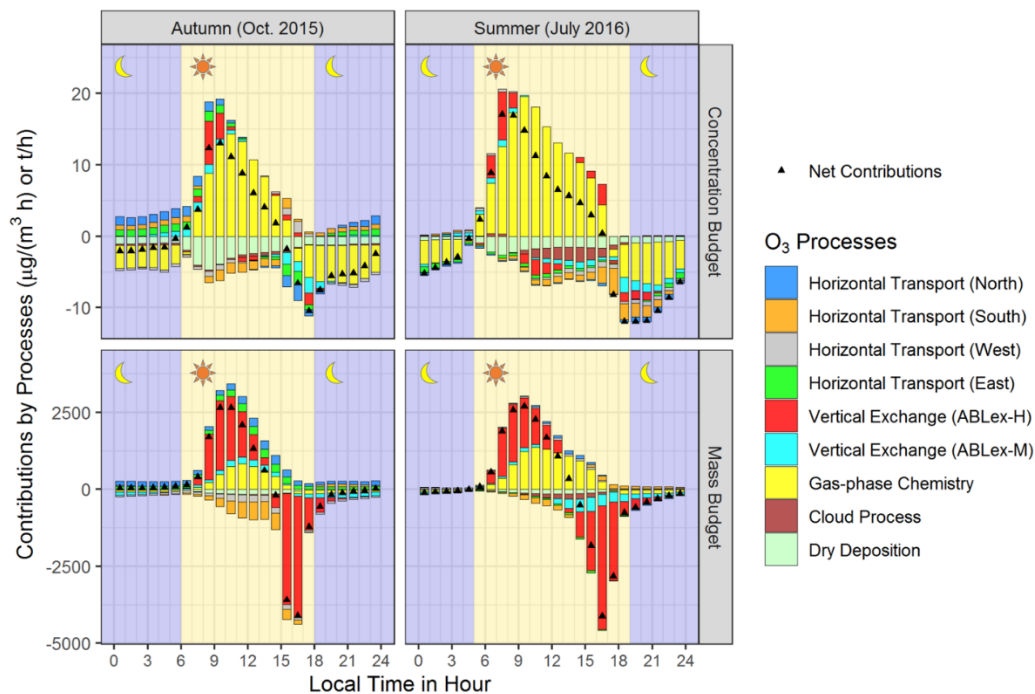
390 of O₃ concentrations in the PRD. In particular, photochemistry led to the rapid formation of O₃ pollution during daytime,

391 rather than transport. Our conclusions agree well with those in earlier studies on the O₃ concentration budget (Lenschow et

392 al., 1981; Hou et al., 2014; Trousdell et al., 2016; Su et al., 2018; Tan et al., 2018; Tan et al., 2019; Trousdell et al., 2019; Yu

393 et al., 2020; Li et al., 2021; Yan et al., 2021).

394



395

396

397 **Figure 34.** Mean diurnal changes of the O₃ concentration budget (upper panels) and mass budget (lower panels) on the polluted days of
 398 representative months in autumn (Oct. 2015; left panels) and summer (July 2016; right panels) within the atmospheric boundary layer of
 399 the Pearl River Delta. The units for the O₃ concentration and mass budgets are μg/(m³ h) and t/h, respectively. Backgrounds in yellow and
 400 dark blue indicate the periods of day and night, daytime and nighttime periods, respectively.

401 3.2 O₃ mass budget

402 The results of the O₃ mass budget are displayed in the lower panels of Fig. 34. The total O₃ mass within the ABL of the PRD
403 increased during the morning hours, decreased rapidly in the afternoon and slowly at the early night, then remained stable
404 until sunrise in both seasons. The change of total O₃ mass agrees well with the ABL diurnal cycle (Lee, 2018) — daytime
405 ABL development (or collapse) and notable O₃ mass increase (or decrease) almost occurred simultaneously, and the
406 negligible changes in O₃ mass during most hours of the night may be linked to the small variations of stable ABL.

407
408 We analysed the contributions of various O₃-related processes in the O₃ mass budget as well, presented as follows:

- 409 • Transport: Unlike the results of the O₃ concentration budget, transport plays a prominent role in the O₃ mass budget.
410 On average, it contributed 78% and 53% to O₃ mass increase during the morning hours of autumn and summer,
411 respectively, and over 90% to O₃ mass decrease during the afternoon hours of both seasons (14:00-18:00 LT in
412 autumn and 14:00-19:00 LT in summer). Most O₃ was transported into or out of the PRD by vertical exchange
413 through the ABL top, especially ABLex-H, which links the diurnal changes of O₃ mass and ABL. That is to say,
414 when the height of ABL rise (drop) rapidly, a big amount of O₃ is transported into (out of) the ABL through the
415 ABLex-H. The contributions of ABLex-~~M-A~~ and horizontal transport to O₃ mass change were relatively limited.
416 However, they ~~indicate correspond~~ well to the characteristics and variations of regional wind fields in the PRD
417 (more details are provided in the next section).
- 418 • Gas-phase chemistry: Gas-phase chemistry (photochemistry) also contributed to the increasing O₃ mass in the
419 daytime, especially in summer. However, its mean contributions during the morning hours (22% in autumn, 47% in
420 summer) were lower than those of transport.
- 421 • Other processes: Dry deposition and cloud process both acted as O₃ sink processes, but with negligible
422 contributions to O₃ mass.

423
424 Based on the above discussions, transport tends to be more important than photochemistry in the O₃ mass budget, which
425 differs from the conclusions of the O₃ concentration budget. The main role of transport, especially ABLex-H, in the O₃ mass
426 budget suggests the marked impacts of the ABL diurnal cycle on regional O₃ pollution. Despite of less notable influence of
427 transport on O₃ concentration increase in comparison to that of photochemistry, massive O₃ being transported into the ABL
428 of the targeted region during the morning hours nearly determines the regional origins of O₃ pollution. Quantified results
429 combining the O₃ mass budget and source apportionment are further discussed in Sect. 4.

430 3.3 Influences of regional wind fields on O₃ pollution: more analyses of transport contributions in O₃ budgets

431 As discussed before, the contributions of horizontal transport and ABLex-~~M-A~~ were relatively limited in the two O₃ budgets.
432 However, they illustrate well the influences of regional wind fields, including the seasonal prevailing winds and local

433 circulations (sea breezes), on O₃ pollution in the PRD. Two main findings from the analyses of these transport contributions
434 are presented below.

435 3.3.1 Transport contributions in autumn: The characteristics of prevailing winds

436 In the PRD, northerly and easterly winds prevail in autumn (as indicated by the wind roses in Fig. S3). Correspondingly, O₃
437 was transported into the PRD through its north and east borders, out of the PRD through the south and west borders, as
438 indicated by the O₃ mass budget (Fig. 34). O₃ masses transported out of the PRD were generally higher than those
439 transported into the PRD during daytime. This is attributed to higher O₃ concentrations in the downwind regions due to O₃
440 production mostly from local emissions. “Low O₃ in, high O₃ out” also explains why horizontal transport led to the net
441 decrease of O₃ concentration during daytime. At night, O₃ was still transported into the region through the north and east
442 borders of the PRD, but these processes contributed to the increase of O₃ concentrations. That is to say, with relatively higher
443 O₃ concentrations compared to those in the NO_x-titrated urban atmosphere, air parcels transported from the upwind outskirts
444 served as the supply to slowdown night-time O₃ level decrease in the PRD due to chemistry and deposition.

445
446 The daytime contributions of ABLex-M-A in the O₃ mass budget also indicate the effects of prevailing northerly winds. The
447 PRD has mountainous regions in the northern, western and eastern outskirts, as well as urban regions with lower altitudes in
448 the central plain (Fig. S6S5). As shown in Fig. S8aS7a-b, the positive contributions of ABLex-M-A through the ABL top (in
449 the z-direction) can be found in the mountainous northern PRD, suggesting that northerly winds resulted in the downward
450 transport of O₃ along the terrain. Daytime ABL heights in urban regions were, in general, higher than those in the
451 surrounding mountainous regions, which is the other reason why O₃ can be transported through the ABL slope (in the x-/y-
452 direction) near the urban-rural interfaces when northerly wind prevailed (Fig. S8eS7c-d). For the O₃ concentration budget,
453 ABLex-M-A contributed to increased O₃ concentration during several hours after sunrise but decreased O₃ concentration in
454 the afternoon. This different effect is attributed to different comparison results between ABL and above-ABL mean O₃
455 concentrations in the two periods (O₃ concentration above the ABL is overall higher than that within the ABL in the
456 morning, while the opposite is for the afternoon; Fig. S4).

458 3.3.2 Transport contributions in summer: The influence of sea breezes

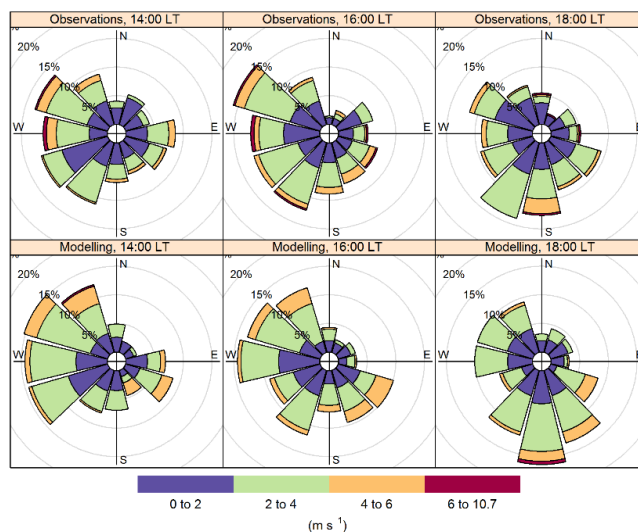
459 Although southerly winds normally prevail in summer in the PRD (Fig. S3), on O₃ polluted days, air parcels from other
460 directions could also influence the region (Qu et al., 2021a). Thus, the mean contribution of horizontal transport to O₃ mass
461 in summer was lower than in autumn. Of particular interest is the variation of the contributions of horizontal transport
462 through the south border of the PRD before and after ~14:00 LT, as indicated by the results of the O₃ mass budget (Fig. 34).
463 Besides, both O₃ budgets suggest notable O₃ mass and concentration decreases due to ABLex-M-A in the afternoon. These
464 phenomena are both related to the influence of sea breezes.

466 Figure 4-5 shows the near-surface wind roses at 14:00, 16:00 and 18:00 LT of O₃ polluted days in July 2016 based on the
467 observational and modelling results in the national meteorological sites within the PRD. At 14:00 LT, the main wind
468 directions were W, SW and NW in both datasets. More S and SE winds occurred in later hours, and they became the
469 prevailing winds at 18:00 LT, suggesting the gradual development of sea breezes in the PRD. Thus, O₃ was originally
470 transported out of the PRD through the south border with negative contributions to O₃ mass; in the late afternoon, sea
471 breezes reversed the directions of O₃ transport, resulting in positive contributions to O₃ mass by horizontal transport through
472 the south border (Fig. 3-4). Moreover, the development of sea breezes is connected to the changes of wind fields not only
473 horizontally, but also vertically. Taking the O₃ polluted day July 24th, 2016 for example, the cross-section of O₃
474 concentrations and wind fields in the PRD at 16:00 LT of the day is shown in Fig. 5-6 (the cross-section is made along the
475 113.2° E longitude, ranging from 26.0° to 20.0° N in latitude). Strong southerly wind and lower O₃ concentrations are found
476 in the southern PRD, indicating the influence of sea breezes during that time. Near the interfaces where sea breezes
477 encountered local air parcels (indicated by the drastic increase in O₃ concentrations from less than 100 µg/m³ to about 100-
478 150 µg/m³), updrafts occurred, suggesting the formation of sea breeze front (Ding et al., 2004; You and Fung, 2019). The
479 front promoted the upward transport of O₃ from the ABL, or considerable O₃ mass decrease due to ABLex-~~MA~~. Both
480 horizontal transport and ABLex-~~MA~~ led to decreased O₃ concentrations, because under the effects of sea breezes, clean air
481 parcels were transported into the region and polluted air parcels were transported out of the region. The influences of sea
482 breezes can also be ~~found-seen~~ in autumn but ~~were-was~~ weaker and occurred later than in summer. Besides, in autumn,
483 horizontal transport through the south border of the PRD contributed to the increase of O₃ concentration at night, indicating
484 the effects of O₃ recirculation from the “O₃ pool” in the bay areas to the south of the PRD (Zeren et al., 2019; Zeren et al.,
485 2022).

486

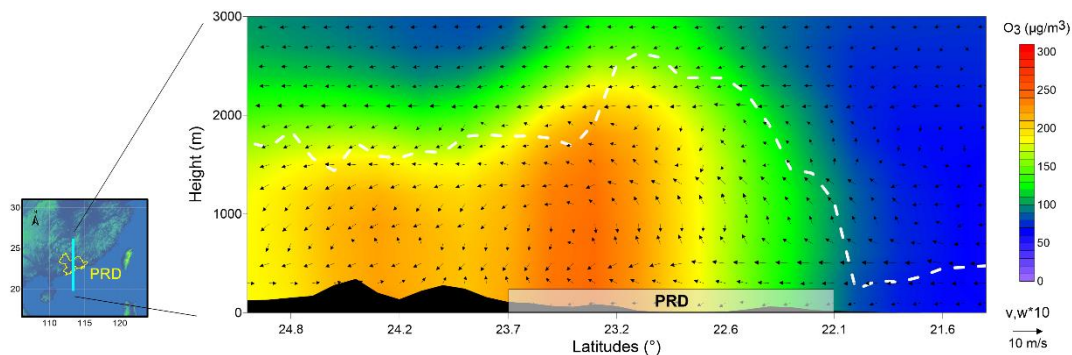
487 Through the calculations and analyses of transport contributions in the two O₃ budgets, the influences of complex transport
488 processes on multiple scales to O₃ concentration and mass can be well identified. These results provide a deeper
489 understanding of how transport influences regional O₃ pollution in the PRD.

490



491

492 **Figure 45.** Wind roses at 14:00, 16:00, and 18:00 local time (LT) of the O₃ polluted days in July 2016 in the Pearl River Delta (PRD).
 493 Observational and modelling wind speeds and directions in 29 national meteorological sites within the PRD were used for this figure.



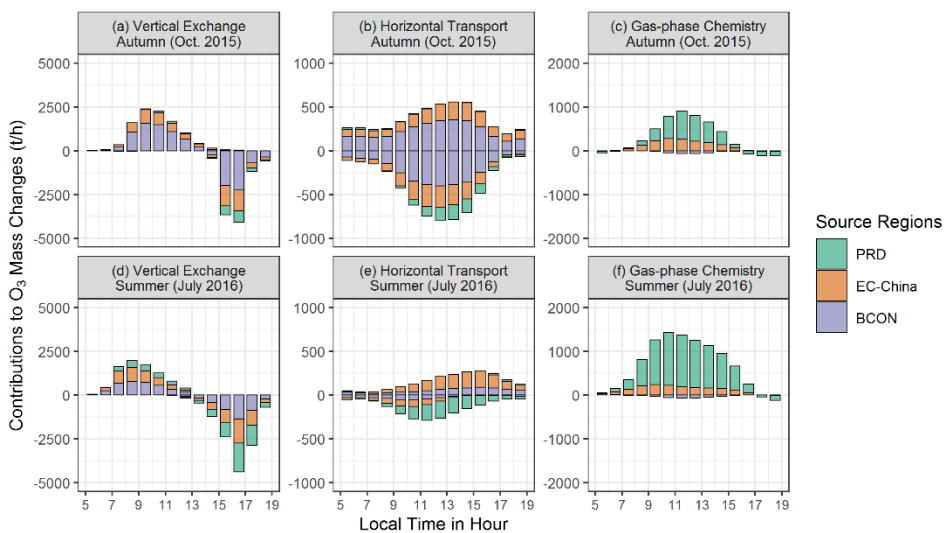
494

495 **Figure 56.** Cross-section of O₃ concentrations (µg/m³) and wind fields at 16:00 local time on July 24th, 2016. The dashed white line
 496 indicates the top of the atmospheric boundary layer. PRD, Pearl River Delta.

497 **4 Effects of transport and photochemistry on the regional origins of O₃**

498 Based on reported publications (Li et al., 2012; Li et al., 2013; Yang et al., 2019; Gao et al., 2020), O₃ in the PRD is mostly
 499 derived from emissions outside the PRD and background O₃, rather than local emissions. This is the same for the O₃ polluted
 500 days in the representative months of autumn and summer in this study, when the contributions of non-local sources account
 501 for on average, 89% and 65% of the O₃ in the PRD, respectively, in 9:00-17:00 LT (55% and 32% contributed by BCON,
 502 34% and 33% contributed by EC-China in the two months; Qu et al., 2021a). To explain why non-local sources are dominant
 503 for O₃ in the PRD, by combining O₃ mass budget calculation with O₃ source apportionment (method introduced in Sect. 2.6),
 504 we identified the regional origins of O₃ mass changes due to vertical exchange through the ABL top, horizontal transport and
 505 gas-phase chemistry (Fig. 67). Here, the contributions of three sources to the O₃ mass increase and decrease were both

506 quantified. But further analyses focus on the results related to O₃ mass increase, because the origins of O₃ in the region are
507 more likely to be influenced by these of “new O₃” transported into and produced within the PRD.



508

509 **Figure 67.** The regional origins of hourly O₃ mass changes contributed by (a,d) vertical exchange through the ABL top, (b,e) horizontal
510 transport, and (c,f) gas-phase chemistry on the polluted days of representative months in autumn (Oct. 2015; a-c) and summer (July 2016;
511 d-f). The results for the time window 5:00-19:00 LT are shown here. PRD, Pearl River Delta; EC-China, East and Central China; BCON,
512 the boundary conditions of d02 modelling, or the contribution of sources outside the d02. Note that the scales are different among the three
513 columns.

514

515 Through vertical exchange through the ABL top, massive non-local O₃ entered into the ABL of the PRD. In the morning-
516 hour O₃ mass increase due to this process, BCON and EC-China accounted for 65% and 31%, respectively, in autumn. By
517 contrast, local emissions only contributed 4% to this transported O₃ during the same period, suggesting that local O₃ was less
518 likely to be recirculated back to the PRD during daytime. In summer, the contribution of local emissions in the O₃ mass
519 transported into the region through vertical exchange was higher than in autumn, reaching 20% during the morning hours.
520 However, non-local sources still dominated the O₃ mass increase due to vertical exchange — the morning-hour contributions
521 in percentage of BCON and EC-China were 42% and 38%, respectively.

522

523 O₃ mass increase due to horizontal transport was connected to the contribution of non-local sources as well. In both seasons,
524 O₃ transported into the PRD originated almost exclusively from EC-China and BCON.

525

526 It is not surprising that most O₃ produced through photochemistry (daytime gas-phase chemistry) was related to local
527 emissions, of which the contributions accounted for 66% and 82% during the daytime of autumn (6:00-18:00 LT) and
528 summer (5:00-19:00 LT), respectively. The contributions of EC-China emissions in the daytime O₃ mass increase reached

529 34% and 18% in the two seasons, respectively, indicating that the influences of non-local O₃ precursor import on local O₃
530 photochemistry are also considerable in the PRD.

531

532 With the results of the O₃ mass budget and the regional origins of O₃ mass increase due to transport and photochemistry, the
533 effects of O₃-related processes on the origins of O₃ can be revealed. Based on the O₃ mass budget, the accumulated morning-
534 hour O₃ mass increase exceeded 10000 tons ~~in the ABL of the PRD~~ for both seasons, which is 6-9 times larger than the
535 original O₃ mass in the ABL of the PRD before sunrise (< 1500 tons). Thus, in the daytime, most O₃ in the ABL-PRD was
536 the “new O₃” contributed by transport and photochemistry, and the origins of O₃ within the region were nearly determined
537 by these of newly transported and produced O₃. By combining the O₃ mass budget and O₃ source apportionment, we
538 identified the O₃ mass increase due to O₃-related processes as local (PRD) and non-local (EC-China and BCON)
539 contributions. According to the results discussed before, high contributions of transport in the morning-hour O₃ mass
540 increase and the dominance of non-local source contributions in this part of new O₃ ensure that non-local sources contributed
541 to most O₃ in the PRD. Moreover, differences in the contributions of O₃-related processes in the O₃ mass budget as well as
542 the origins of morning-hour O₃ mass increase lead to varied origins of O₃ in the region. For instance, when comparing the
543 results of O₃ source apportionment in the two seasons, we found that the contributions of non-local sources (local emissions)
544 to O₃ were lower (higher) in summer than in autumn. It can be attributed to the combined effects of increased
545 photochemistry contributions (or decreased transport contributions) in the O₃ mass increase, and reduced non-local source
546 contributions in both transported and chemically produced O₃ in summer. Collectively, these changes lead to reduced non-
547 local contributions (or higher local contributions) to O₃.

548

549 By influencing O₃ mass increase and its regional origins, transport and photochemistry determine the results of O₃ source
550 apportionment within the region. Specifically, transport (mainly ABLex-H) brings massive non-local O₃ into the region in
551 the morning, explaining why most O₃ in the PRD is derived from non-local sources. However, accompanied with the
552 simultaneous rapid increase of ABL volumes, this process has a relatively limited contribution to O₃ concentration increase
553 in comparison to photochemistry. The O₃ concentration budget only concerns the influence of O₃-related processes on the
554 variations of O₃ concentration, thus it fails to illustrate the effect of transport on the regional origins of O₃. Our results
555 highlight the difference between the O₃ concentration and mass budgets, which may result in distinct understandings about
556 the role of transport and photochemistry in regional O₃ pollution. However, ~~T~~o completely illustrate the effects of two O₃-
557 related processes on regional O₃ pollution, insights from both O₃ budgets are required.

558 **5 Conclusion and outlook**

559 To effectively alleviate O₃ pollution, it is important to understand the respective role of transport and photochemistry in
560 regional O₃ pollution. The O₃ concentration budget is widely used to quantify the contributions of these O₃-related processes

561 to the variations of O₃ concentrations, and it often concludes that photochemistry is the main contributor to the aggravation
562 of O₃ pollution. However, it does not explain why most of the O₃ is transported from the outside regions as indicated by O₃
563 source apportionment studies. To comprehensively illustrate the effects of transport and photochemistry on regional O₃
564 pollution, based on the modelling results of WRF-CMAQ, this study presents a method to quantify not only the O₃
565 concentration budget, but also the O₃ mass budget, in which the contributions of O₃-related processes (including transport
566 and photochemistry) to the variations of mean O₃ concentrations and total O₃ mass within the ABL of the PRD are separately
567 identified. The different effects of transport on O₃ concentration and mass were considered in the above calculations. The O₃
568 concentration budget in the PRD reveals that gas-phase chemistry, including daytime photochemistry and night-time O₃
569 titration/depletion, drives the variations of O₃ concentration. Particularly, photochemistry contributed 74% and 95% to the
570 O₃ concentration increase in the morning hours of autumn and summer months, respectively. In contrast, transport,
571 especially the vertical exchange through the ABL top, is the main process contributing to the O₃ mass increase in the
572 morning (78% and 53% in autumn and summer, respectively) and decrease in the afternoon (> 90%). The diurnal changes of
573 transport contributions in the two O₃ budgets are closely connected to the variations of the ABL and regional wind fields,
574 including the seasonal prevailing winds and local circulations (sea breezes), in the PRD. ~~Although massive~~ O₃, mostly
575 derived from non-local sources, being transported into the ABL in the morning has a relatively limited influence on the O₃
576 concentration increase (25% and 5% in autumn and summer, respectively) compared to photochemistry because of the rapid
577 change of ABL volumes at the same time. However, this process nearly determines the dominance of non-local source
578 contributions for daytime O₃ in the PRD. The two O₃ budgets show notable differences, but together they provide a more
579 complete overview ~~on~~ of the effects of transport and photochemistry on regional O₃ pollution.

580

581 It should be noted that the conclusions in this study apply not only to O₃, but also to other pollutants with moderately long
582 atmospheric lifetimes, including fine particulate matter and some of its components. In theory, transport and chemical
583 transformations are both important processes for these pollutants. However, transport has different effects on the
584 concentration and mass of pollutants ~~at~~ on an hourly scale, which is similar to the discussion in Sect. 2.4. Furthermore,
585 besides regional origins, the difference between the two budgets may also contribute to the inconsistency of other
586 characteristics of pollutants, such as the contributions of different reaction pathways and sensitivities to precursor emissions,
587 identified by the concentration budget and mass-based methods. When large quantities of pollutants with different
588 characteristics are transported into the region, the variation of their concentrations is often not perceptible and thus neglected
589 in the concentration budget. However, as indicated by this study, the transport processes are likely to change or even
590 determine the characteristics of pollutants within the region. Therefore, we suggest that attention should be paid to selecting
591 a proper budget type and using correct budget calculation methods in related research. ~~Insights from both concentration and~~
592 ~~mass budgets are necessary~~ But to fully reveal the effects of transport, chemistry and other related processes on regional
593 pollution, insights from both concentration and mass budgets are necessary.

594

595 Uncertainty remains in the calculated O₃ budgets, which is partly related to the biases in the modelling results. Therefore,
596 supporting observations are essential for future research. Recent progress in observational techniques (Zhao et al., 2021;
597 Zhou et al., 2021) has enabled three-dimensional measurements of meteorological parameters and O₃ concentrations with
598 high spatiotemporal resolution and coverage. These data can be used not only for the model validation of key parameters in
599 budget calculations, but also for the comparisons between observation- and modelling-based contributions by various O₃-
600 related processes in O₃ budgets (Kaser et al., 2017). The comparison of contributions by O₃-related processes is indicative of
601 the main uncertainties in O₃ pollution modelling, and is therefore also important for further model developments.

602

603 The present study concluded that transport and gas-phase chemistry play the main role in the O₃ mass and concentration
604 budgets, respectively. As a consequence of our assessment, ~~what should policy makers do to effectively alleviate regional O₃~~
605 ~~pollution?the following is suggested for policy-makers.~~ For areas where non-local emissions notably contribute to O₃,
606 emission reduction in the upwind regions ~~will can effectively~~ reduce the overall O₃ concentrations effectively, which is a
607 crucial step towards the long-term improvement of regional air quality. However, for short-term air pollution control, this
608 strategy is not efficient because emission reduction in upwind regions may need to start days earlier before the polluted
609 periods. In contrast, reducing local emissions is expected to ~~efficiently~~ lower the rapid daytime O₃ concentration increase
610 efficiently and, thereby, O₃ peak levels in the short term, as highlighted by the O₃ concentration budget. The choice of the
611 better strategy to be applied should depend on the specific objectives of O₃ control (mean levels vs. peak levels; long-term
612 vs. short-term), which are set based on a more in-depth understanding of O₃ effects on human health, crop yields and
613 ecosystems. More efforts are required to systematically evaluate the effects of different emission reduction strategies on
614 alleviating the detrimental effects of O₃.

615

616 *Data availability.* The source codes of WRF and CMAQ are available at the site
617 https://www2.mmm.ucar.edu/wrf/users/download/get_sources.html and <https://www.cmascenter.org/cmaq/>, respectively.
618 FNL meteorological input files were downloaded from the site <https://rda.ucar.edu/datasets/ds083.2/>. MEIC v1.3
619 anthropogenic emission inventory is available at http://meicmodel.org/?page_id=560. The source codes of MEGAN can be
620 found at <https://bai.ess.uci.edu/megan/data-and-code>. IAGOS dataset used in model validation was searched and downloaded
621 from <http://iagos-data.fr>, which includes all profiles measured in flights taking off from and landing in Hong Kong during
622 the two representative months. We also provided the initial Fortran code used in ozone budget calculations and hourly O₃
623 concentration and mass budget results in the two representative months (the initial data of Fig. 34) at
624 <https://doi.org/10.5281/zenodo.6259253>.

625

626 *Author contributions.* KQ, XW and YZ designed the study. KQ, XW, TX did the simulations using the WRF-CMAQ model.
627 JS, LZ and YZ provided observational results for model validation. KQ, XW, XC, YY, XJ and YZ developed the post-

628 processing tool *flux_4d_cal*, conducted and analysed O₃ budget results. KQ, XW, MV, MK, GB and YZ wrote and/or revised
629 this paper, with critical feedbacks from all other authors.

630

631 *Competing interests.* One of the authors is a member of the editorial board of Atmospheric Chemistry and Physics, and the
632 peer-review process was guided by an independent editor. The authors declare no other conflict of interest.

633

634 *Acknowledgements.* This study was supported by the National Key Research and Development Program of China (grant No.
635 2018YFC0213204), the National Science and Technology Pillar Program of China (grant No. 2014BAC21B01) and the co-
636 funded DFG-NSFC Sino-German AirChanges project (grant No. 448720203).

637

638 **References**

- 639 Ainsworth, E. A.: Understanding and improving global crop response to ozone pollution, *Plant J.*, 90, 886–897,
640 <https://doi.org/10.1111/tpj.13298>, 2017.
- 641 Bates, K. H. and Jacob, D. J.: An expanded definition of the odd oxygen family for tropospheric ozone budgets: Implications
642 for ozone lifetime and stratospheric influence, *Geophys. Res. Lett.*, 47, e2019GL084486,
643 <https://doi.org/10.1029/2019GL084486>, 2019.
- 644 Boian, C. and Andrade, M. D. F.: Characterization of ozone transport among metropolitan regions, *Rev. Bras. Meteorol.*, 27,
645 229–242, <https://doi.org/10.1590/S0102-77862012000200009>, 2012.
- 646 Carter, W. P. L.: Development of the SAPRC-07 chemical mechanism, *Atmos. Environ.*, 44, 5324–5335,
647 <https://doi.org/10.1016/j.atmosenv.2010.01.026>, 2010.
- 648 Chang, X., Wang, S., Zhao, B., Cai, S., and Hao, J.: Assessment of inter-city transport of particulate matter in the Beijing–
649 Tianjin–Hebei region, *Atmos. Chem. Phys.*, 18, 4843–4858, <https://doi.org/10.5194/acp-18-4843-2018>, 2018.
- 650 Clappier, A., Belis, C. A., Pernigotti, D., and Thunis, P.: Source apportionment and sensitivity analysis: two methodologies
651 with two different purposes, *Geosci. Model Dev.*, 10, 4245–4256, <https://doi.org/10.5194/gmd-10-4245-2017>, 2017.
- 652 Ding, A., Wang, T., Zhao, M., Wang, T. J., and Li, Z. K.: Simulation of sea-land breezes and a discussion of their
653 implications on the transport of air pollution during a multi-day ozone episode in the Pearl River Delta of China,
654 *Atmos. Environ.*, 38, 6737–6750, <https://doi.org/10.1016/j.atmosenv.2004.09.017>, 2004.
- 655 Fishman, J., Wozniak, A. E., and Creilson, J. K.: Global distribution of tropospheric ozone from satellite measurements
656 using the empirically corrected tropospheric ozone residual technique: Identification of the regional aspects of air
657 pollution, *Atmos. Chem. Phys.*, 3, 893–907, <https://doi.org/10.5194/acp-3-893-2003>, 2003.
- 658 Fleming, Z. L., Doherty, R. M., von Schneidemesser, E., Malley, C. S., Cooper, O. R., Pinto, J. P., Colette, A., Xu, X. B.,
659 Simpson, D., Schultz, M. G., Lefohn, A. S., Hamad, S., Moolla, R., Solberg, S., and Feng, Z. Z.: Tropospheric ozone
660 assessment report: Present-day ozone distribution and trends relevant to human health, *Elementa-Sci. Anthropol.*, 6, 12,
661 <https://doi.org/10.1525/elementa.273>, 2018.
- 662 Fowler, D., Brimblecombe, P., Burrows, J., Heal, M. R., Grennfelt, P., Stevenson, D. S., Jowett, A., Nemitz, E., Coyle, M.,
663 Liu, X., Chang, Y., Fuller, G. W., Sutton, M. A., Klimont, Z., Unsworth, M. H., and Vieno, M.: A chronology of global
664 air quality, *Philos. T. R. Soc. A*, 378, 20190314, <https://doi.org/10.1098/rsta.2019.0314>, 2020.
- 665 Gao, M., Gao, J., Zhu, B., Kumar, R., Lu, X., Song, S., Zhang, Y., Jia, B., Wang, P., Beig, G., Hu, J., Ying, Q., Zhang, H.,
666 Sherman, P., and McElroy, M. B.: Ozone pollution over China and India: seasonality and sources, *Atmos. Chem. Phys.*,
667 20, 4399–4414, <https://doi.org/10.5194/acp-20-4399-2020>, 2020.
- 668 Gao, X., Deng, X., Tan, H., Wang, C., Wang, N., and Yue, D.: Characteristics and analysis on regional pollution process and
669 circulation weather types over Guangdong Province, *Acta Scientiae Circumstantiae (in Chinese)*, 38(5), 1708–1716,
670 <https://doi.org/10.13671/j.hjkxxb.2017.0473>, 2018.

671 Guo, J. J., Fiore, A. M., Murray, L. T., Jaffe, D. A., Schnell, J. L., Moore, C. T., and Milly, G. P.: Average versus high
672 surface ozone levels over the continental USA: model bias, background influences, and interannual variability, *Atmos.*
673 *Chem. Phys.*, 18, 12123–12140, <https://doi.org/10.5194/acp-18-12123-2018>, 2018.

674 He, K.: Multi-resolution Emission Inventory for China (MEIC): model framework and 1990-2010 anthropogenic emissions,
675 American Geophysical Union, Fall Meeting 2012, 3–7 December 2012, San Francisco, USA, A32B-05, 2012.

676 Hou, X., Zhu, B., Kang, H., and Gao, J.: Analysis of seasonal ozone budget and spring ozone latitudinal gradient variation in
677 the boundary layer of the Asia-Pacific region, *Atmos. Environ.*, 94, 734–741,
678 <https://doi.org/10.1016/j.atmosenv.2014.06.006>, 2014.

679 Hu, J., Li, Y., Zhao, T., Liu, J., Hu, X.-M., Liu, D., Jiang, Y., Xu, J., and Chang, L.: An important mechanism of regional O₃
680 transport for summer smog over the Yangtze River Delta in eastern China, *Atmos. Chem. Phys.*, 18, 16239–16251,
681 <https://doi.org/10.5194/acp-18-16239-2018>, 2018.

682 Janssen, R. H. H. and Pozzer, A.: Description and implementation of a MiXed Layer model (MXL, v1.0) for the dynamics of
683 the atmospheric boundary layer in the Modular Earth Submodel System (MESSy), *Geosci. Model Dev.*, 8, 453–471,
684 <https://doi.org/10.5194/gmd-8-453-2015>, 2015.

685 Jin, X., Cai, X., Huang, Q., Wang, X., Song, Y., and Zhu, T.: Atmospheric boundary layer—free troposphere air exchange in
686 the North China Plain and its impact on PM_{2.5} pollution, *J. Geophys. Res.-Atmos.*, 126(9), e2021JD034641,
687 <https://doi.org/10.1029/2021JD034641>, 2021.

688 Kaser, L., Patton, E. G., Pfister, G. G., Weinheimer, A. J., Montzka, D. D., Flocke, F., Thompson, A. M., Stauffer, R. M.,
689 and Halliday, H. S.: The effect of entrainment through atmospheric boundary layer growth on observed and modeled
690 surface ozone in the Colorado Front Range, *J. Geophys. Res.-Atmos.*, 122, 6075–6093,
691 <https://doi.org/10.1002/2016JD026245>, 2017.

692 Laughner, J. L. and Cohen, R. C.: Direct observation of changing NO_x lifetime in North American cities, *Science*, 366, 723–
693 727, <https://doi.org/10.1126/science.aax6832>, 2019.

694 Lee, X.: *Fundamentals of Boundary-Layer Meteorology*, Springer Atmospheric Sciences., 2018.

695 Lelieveld, J., Hoor, P., Jöckel, P., Pozzer, A., Hadjinicolaou, P., Cammas, J.-P., and Beirle, S.: Severe ozone air pollution in
696 the Persian Gulf region, *Atmos. Chem. Phys.*, 9, 1393–1406, <https://doi.org/10.5194/acp-9-1393-2009>, 2009.

697 Lenschow, D. H., Pearson, R., and Stankov, B. B.: Estimating the ozone budget in the boundary layer by use of aircraft
698 measurements of ozone eddy flux and mean concentration, *J. Geophys. Res.*, 86, 7291–7297,
699 <https://doi.org/10.1029/JC086iC08p07291>, 1981.

700 Li, L., Xie, F., Li, J., Gong, K., Xie, X., Qin, Y., Qin, M., and Hu, J.: Diagnostic analysis of regional ozone pollution in
701 Yangtze River Delta, China: A case study in summer 2020, *Sci. Total Environ.*, 812, 151511,
702 <https://doi.org/10.1016/j.scitotenv.2021.151511>, 2021.

703 Li, M., Zhang, Q., Kurokawa, J.-I., Woo, J.-H., He, K., Lu, Z., Ohara, T., Song, Y., Streets, D. G., Carmichael, G. R., Cheng,
704 Y., Hong, C., Huo, H., Jiang, X., Kang, S., Liu, F., Su, H., and Zheng, B.: MIX: a mosaic Asian anthropogenic emission

705 inventory under the international collaboration framework of the MICS-Asia and HTAP, *Atmos. Chem. Phys.*, 17, 935–
706 963, <https://doi.org/10.5194/acp-17-935-2017>, 2017.

707 Li, Y., Lau, A. K. H., Fung, J. C. H., Ma, H., and Tse, Y.: Systematic evaluation of ozone control policies using an Ozone
708 Source Apportionment method, *Atmos. Environ.*, 76, 136–146, <https://doi.org/10.1016/j.atmosenv.2013.02.033>, 2013.

709 Li, Y., Lau, A. K. H., Fung, J. C. H., Zheng, J. Y., Zhong, L. J., and Louie, P. K. K.: Ozone source apportionment (OSAT) to
710 differentiate local regional and super-regional source contributions in the Pearl River Delta region, China, *J. Geophys.*
711 *Res.-Atmos.*, 117, D15305, <http://doi.org/10.1029/2011JD017340>, 2012.

712 Liu, F., Beirle, S., Zhang, Q., Dörner, S., He, K., and Wagner, T.: NO_x lifetimes and emissions of cities and power plants in
713 polluted background estimated by satellite observations, *Atmos. Chem. Phys.*, 16, 5283–5298,
714 <https://doi.org/10.5194/acp-16-5283-2016>, 2016.

715 Liu, H. L., Zhang, M. G., and Han, X.: A review of surface ozone source apportionment in China, *Atmos. Ocean. Sci. Lett.*,
716 13, 470–484, <https://doi.org/10.1080/16742834.2020.1768025>, 2020.

717 Liu, P., Zhang, Y., Yu, S. C., and Schere, K. L.: Use of a Process Analysis tool for diagnostic study on fine particulate matter
718 predictions in the U.S. Part II: Process Analysis and sensitivity simulations, *Atmos. Pollut. Res.*, 2, 61–71,
719 <https://doi.org/10.5094/APR.2011.008>, 2011.

720 Massagué, J., Carnerero, C., Escudero, M., Baldasano, J. M., Alastuey, A., and Querol, X.: 2005–2017 ozone trends and
721 potential benefits of local measures as deduced from air quality measurements in the north of the Barcelona
722 metropolitan area, *Atmos. Chem. Phys.*, 19, 7445–7465, <https://doi.org/10.5194/acp-19-7445-2019>, 2019.

723 Mills, G., Wagg, S., and Harmens, H.: Ozone pollution: impacts on ecosystem services and biodiversity (CEH Project no.
724 C04062, C04325), Bangor, UK, NERC/Centre for Ecology & Hydrology, 2013.

725 Myriokefalitakis, S., Daskalakis, N., Fanourgakis, G. S., Voulgarakis, A., Krol, M. C., de Brugh, J. A., and Kanakidou, M.:
726 Ozone and carbon monoxide budgets over the Eastern Mediterranean, *Sci. Total Environ.*, 563, 40–52,
727 <https://doi.org/10.1016/j.scitotenv.2016.04.061>, 2016.

728 Naik, V., Szopa, S., Adhikary, B., Artaxo, P., Berntsen, T., Collins, W. D., Fuzzi, S., Gallardo, L., Kiendler Scharr, A.,
729 Klimont, Z., Liao, H., Unger, N., and Zanis, P.: Short-Lived Climate Forcers, in: *Climate Change 2021: The Physical*
730 *Science Basis. Contribution of Working Group I to the Sixth Assessment Report of the Intergovernmental Panel on*
731 *Climate Change*, edited by: Masson-Delmotte, V., Zhai, P., Pirani, A., Connors, S. L., Péan, C., Berger, S., Caud, N.,
732 Chen, Y., Goldfarb, L., Gomis, M. I., Huang, M., Leitzell, K., Lonnoy, E., Matthews, J. B. R., Maycock, T. K.,
733 Waterfield, T., Yelekçi, O., Yu, R., and Zhou, B., Cambridge University Press, Cambridge, United Kingdom and New
734 York, NY, USA, 817–922, <https://doi.org/10.1017/9781009157896.008>, 2021.

735 Novel, D. P.: The OTC challenge: Adding VOC controls in the northeast, *J. Air Waste Manag. Assoc.*, 42(8), 1053–1056,
736 <https://doi.org/10.1080/10473289.1992.10467050>, 1992.

737 Pay, M. T., Gangoiiti, G., Guevara, M., Napelenok, S., Querol, X., Jorba, O., and Pérez García-Pando, C.: Ozone source
738 apportionment during peak summer events over southwestern Europe, *Atmos. Chem. Phys.*, 19, 5467–5494,
739 <https://doi.org/10.5194/acp-19-5467-2019>, 2019.

740 Petzold, A., Thouret, V., Gerbig, C., Zahn, A., Brenninkmeijer, C. A. M., Gallagher, M., Hermann, M., Pontaud, M., Ziereis,
741 H., Boulanger, D., Marshall, J., Nédélec, P., Smit, H. G. J., Friess, U., Flaud, J.-M., Wahner, A., Cammas, J.-P., Volz-
742 Thomas, A. and IAGOS TEAM: Global-scale atmosphere monitoring by in-service aircraft—current achievements and
743 future prospects of the European Research Infrastructure IAGOS, *Tellus B*, 67, 28452,
744 <https://doi.org/10.3402/tellusb.v67.28452>, 2015.

745 Qu, K., Wang, X., Xiao, T., Shen, J., Lin, T., Chen, D., He, L., Huang, X., Zeng, L., Lu, K., Ou, Y., and Zhang, Y.: Cross-
746 regional transport of PM_{2.5} nitrate in the Pearl River Delta, China: Contributions and mechanisms, *Sci. Total Environ.*,
747 753, 142439, <https://doi.org/10.1016/j.scitotenv.2020.142439>, 2021b.

748 Qu, K., Wang, X., Yan, Y., Shen, J., Xiao, T., Dong, H., Zeng, L., and Zhang, Y.: A comparative study to reveal the
749 influence of typhoons on the transport, production and accumulation of O₃ in the Pearl River Delta, China, *Atmos.*
750 *Chem. Phys.*, 21, 11593–11612, <https://doi.org/10.5194/acp-21-11593-2021>, 2021a.

751 Reid, N., Yap, D., and Bloxam, R.: The potential role of background ozone on current and emerging air issues: An overview,
752 *Air Qual. Atmos. Health*, 1, 19–29, <https://doi.org/10.1007/s11869-008-0005-z>, 2008.

753 Schultz, M. G., Schröder, S., Lyapina, O., Cooper, O., Galbally, I., Petropavlovskikh, I., Von Schneidmesser, E., Tanimoto,
754 H., Elshorbany, Y., Naja, M., Seguel, R., Dauert, U., Eckhardt, P., Feigenspahn, S., Fiebig, M., Hjellbrekke, A.-G.,
755 Hong, Y.-D., Kjeld, P. C., Koide, H., Lear, G., Tarasick, D., Ueno, M., Wallasch, M., Baumgardner, D., Chuang, M.-T.,
756 Gillett, R., Lee, M., Molloy, S., Moolla, R., Wang, T., Sharps, K., Adame, J. A., Ancellet, G., Apadula, F., Artaxo, P.,
757 Barlasina, M., Bogucka, M., Bonasoni, P., Chang, L., Colomb, A., Cuevas, E., Cupeiro, M., Degorska, A., Ding, A.,
758 Fröhlich, M., Frolova, M., Gadhavi, H., Gheusi, F., Gilge, S., Gonzalez, M. Y., Gros, V., Hamad, S. H., Helmig, D.,
759 Henriques, D., Hermansen, O., Holla, R., Huber, J., Im, U., Jaffe, D. A., Komala, N., Kubistin, D., Lam, K.-S., Laurila,
760 T., Lee, H., Levy, I., Mazzoleni, C., Mazzoleni, L., McClure-Begley, A., Mohamad, M., Murovic, M., Navarro-Comas,
761 M., Nicodim, F., Parrish, D., Read, K. A., Reid, N., Ries, L., Saxena, P., Schwab, J. J., Scorgie, Y., Senik, I.,
762 Simmonds, P., Sinha, V., Skorokhod, A., Spain, G., Spangl, W., Spoor, R., Springston, S. R., Steer, K., Steinbacher, M.,
763 Suharguniyawan, E., Torre, P., Trickl, T., Weili, L., Weller, R., Xu, X., Xue, L., and Zhiqiang, M.: Tropospheric ozone
764 assessment report: Database and metrics data of global surface ozone observations, *Elementa-Sci. Anthropol.*, 5, 58,
765 <https://doi.org/10.1525/elementa.244>, 2017.

766 Seinfeld, J. H. and Pandis, S. N.: *Atmospheric chemistry and physics: from air pollution to climate change*, John Wiley &
767 Sons, 2016.

768 Sinclair, V. A., Belcher, S. E., and Gray, S. L.: Synoptic controls on boundary-layer characteristics, *Bound.-Layer Meteorol.*,
769 134, 387–409, <https://doi.org/10.1007/s10546-009-9455-6>, 2010.

770 Sitch, S., Cox, P. M., Collins, W. J., and Huntingford, C.: Indirect radiative forcing of climate change through ozone effects
771 on the land-carbon sink, *Nature*, 448, 791–795, <https://doi.org/10.1038/nature06059>, 2007.

772 Stevenson, D. S., Dentener, F. J., Schultz, M. G., Ellingsen, K., van Noije, T. P. C., Wild, O., Zeng, G., Amann, M.,
773 Atherton, C. S., Bell, N., Bergmann, D. J., Bey, I., Butler, T., Cofala, J., Collins, W. J., Derwent, R. G., Doherty, R. M.,
774 Drevet, J., Eskes, H. J., Fiore, A. M., Gauss, M., Hauglustaine, D. A., Horowitz, L. W., Isaksen, I. S. A., Krol, M. C.,
775 Lamarque, J.-F., Lawrence, M. G., Montanaro, V., Müller, J.-F., Pitari, G., Prather, M. J., Pyle, J. A., Rast, S.,
776 Rodriguez, J. M., Sanderson, M. G., Savage, N. H., Shindell, D. T., Strahan, S. E., Sudo, K., and Szopa, S.: Multimodel
777 ensemble simulations of present-day and near-future tropospheric ozone, *J. Geophys. Res.*, 111, D08301,
778 <https://doi.org/10.1029/2005JD006338>, 2006.

779 Su, R., Lu, K. D., Yu, J. Y., Tan, Z. F., Jiang, M. Q., Li, J., Xie, S. D., Wu, Y. S., Zeng, L. M., Zhai, C. Z., and Zhang, Y. H.:
780 Exploration of the formation mechanism and source attribution of ambient ozone in Chongqing with an observation-
781 based model, *Sci. China Earth Sci.*, 61, 23–32, <https://doi.org/10.1007/s11430-017-9104-9>, 2018.

782 Tan, Z., Lu, K., Jiang, M., Su, R., Dong, H., Zeng, L., Xie, S., Tan, Q., and Zhang, Y.: Exploring ozone pollution in
783 Chengdu, southwestern China: A case study from radical chemistry to O₃-VOC-NO_x sensitivity, *Sci. Total Environ.*,
784 636, 775–786, <https://doi.org/10.1016/j.scitotenv.2018.04.286>, 2018.

785 Tan, Z., Lu, K., Jiang, M., Su, R., Wang, H., Lou, S., Fu, Q., Zhai, C., Tan, Q., Yue, D., Chen, D., Wang, Z., Xie, S., Zeng,
786 L., and Zhang, Y.: Daytime atmospheric oxidation capacity in four Chinese megacities during the photochemically
787 polluted season: a case study based on box model simulation, *Atmos. Chem. Phys.*, 19, 3493–3513,
788 <https://doi.org/10.5194/acp-19-3493-2019>, 2019.

789 Thunis, P., Clappier, A., Tarrason, L., Cuvelier, C., Monteiro, A., Pisoni, E., Wesseling, J., Belis, C. A., Pirovano, G.,
790 Janssen, S., Guerreiro, C., and Peduzzi, E.: Source apportionment to support air quality planning: Strengths and
791 weaknesses of existing approaches, *Environ. Int.*, 130, 104825, <https://doi.org/10.1016/j.envint.2019.05.019>, 2019.

792 Trousdell, J. F., Caputi, D., Smoot, J., Conley, S. A., and Faloona, I. C.: Photochemical production of ozone and emissions
793 of NO_x and CH₄ in the San Joaquin Valley, *Atmos. Chem. Phys.*, 19, 10697–10716, <https://doi.org/10.5194/acp-19-10697-2019>, 2019.

794

795 Trousdell, J. F., Conley, S. A., Post, A., and Faloona, I. C.: Observing entrainment mixing, photochemical ozone production,
796 and regional methane emissions by aircraft using a simple mixed-layer framework, *Atmos. Chem. Phys.*, 16, 15433–
797 15450, <https://doi.org/10.5194/acp-16-15433-2016>, 2016.

798

799 Vilà-Guerau De Arellano, J., van Heerwaarden, C. C., van Stratum, B. J. H., and van den Dries, K.: *Atmospheric Boundary
Layer: Integrating Air Chemistry and Land Interactions*, Cambridge University Press, New York, 2015.

800 Yan, F., Gao, Y., Ma, M., Liu, C., Ji, X., Zhao, F., Yao, X., and Gao, H.: Revealing the modulation of boundary conditions
801 and governing processes on ozone formation over northern China in June 2017, *Environ. Pollut.*, 272, 115999,
802 <https://doi.org/10.1016/j.envpol.2020.115999>, 2021.

803 Yang, L., Wang, X., and Chen, Q.: New method for investigating regional interactions of air pollutants (in Chinese), *Acta*
804 *Sci. Circumstantiae*, 32(3), 528-536, <https://doi.org/10.13671/j.hjkxxb.2012.03.012>, 2012.

805 Yang, W., Chen, H., Wang, W., Wu, J., Li, J., Wang, Z., Zheng, J., and Chen, D.: Modeling study of ozone source
806 apportionment over the Pearl River Delta in 2015, *Environ. Pollut.*, 253, 393-402,
807 <https://doi.org/10.1016/j.envpol.2019.06.091>, 2019.

808 You, C., and Fung, J. C. H.: Characteristics of the sea-breeze circulation in the Pearl River Delta region and its dynamical
809 diagnosis. *Journal of Applied Meteorology and Climatology*, 58(4), 741-755, <https://doi.org/10.1175/JAMC-D-18->
810 0153.1, 2019.

811 Yu, D., Tan, Z., Lu, K., Ma, X., Li, X., Chen, S., Zhu, B., Lin, L., Li, Y., Qiu, P., Yang, X., Liu, Y., Wang, H., He, L.,
812 Huang, X., and Zhang, Y.: An explicit study of local ozone budget and NO_x-VOCs sensitivity in Shenzhen China,
813 *Atmos. Environ.*, 224, 117304, <https://doi.org/10.1016/j.atmosenv.2020.117304>, 2020.

814 Zeren, Y., Guo, H., Lyu, X., Jiang, F., Wang, Y., Liu, X., Zeng, L., Li, M., and Li, L.: An Ozone “Pool” in South China:
815 Investigations on Atmospheric Dynamics and Photochemical Processes Over the Pearl River Estuary, *J. Geophys. Res.*,
816 124, 12340–12355, <https://doi.org/10.1029/2019jd030833>, 2019.

817 Zeren, Y., Zhou, B., Zheng, Y., Jiang, F., Lyu, X., Xue, L., Wang, H., Liu, X., and Guo, H.: Does Ozone Pollution Share the
818 Same Formation Mechanisms in the Bay Areas of China?, *Environ. Sci. Tech.*, 56(20), 14326-14337,
819 <https://doi.org/10.1021/acs.est.2c05126>, 2022.

820 Zhang, J. J., Wei, Y., and Fang, Z.: Ozone pollution: A major health hazard worldwide, *Front. Immunol.*, 10, 2518,
821 <https://doi.org/10.3389/fimmu.2019.02518>, 2019.

822 Zhao, R., Hu, Q., Sun, Z., Wu, Y., Xing, C., Liu, H., and Liu, C.: Review of space and ground integrated remote sensing for
823 air pollutants (in Chinese). *Res. Environ. Sci.*, 34(1), 28-40. <https://doi.org/10.13198/j.issn.1001-6929.2020.11.25>,
824 2021.

825 Zhao, W., Tang, G., Yu, H., Yang, Y., Wang, Y., Wang, L., An, J., Gao, W., Hu, B., Cheng, M., An, X., Li, X., and Wang,
826 Y.: Evolution of boundary layer ozone in Shijiazhuang, a suburban site on the North China Plain, *J. Environ. Sci.*, 83,
827 152–160, <https://doi.org/10.1016/j.jes.2019.02.016>, 2019.

828 Zhou, B., Zhang, S., Xue, R., Li, J., and Wang, S.: A review of Space-Air-Ground integrated remote sensing techniques for
829 atmospheric monitoring, *J. Environ. Sci.*, <https://doi.org/10.1016/j.jes.2021.12.008>, 2021.

830